

Charge distribution and magnetism in bilayer $\text{La}_3\text{Ni}_2\text{O}_7$: a hybrid functional study

Kateryna Foyevtsova,^{1,2,3,4} Ilya Elfimov,^{3,4} and George A. Sawatzky^{3,4}

¹*Department of Physics and Astronomy, University of Notre Dame, Notre Dame, IN, USA*

²*Stavropoulos Center for Complex Quantum Matter,
University of Notre Dame, Notre Dame, IN, USA*

³*Department of Physics & Astronomy, University of British Columbia, Vancouver, British Columbia V6T 1Z1, Canada*

⁴*Stewart Blusson Quantum Matter Institute, University of British Columbia, Vancouver, British Columbia V6T 1Z4, Canada*

(Dated: July 14, 2025)

An accurate understanding of the ground state electronic properties of $\text{La}_3\text{Ni}_2\text{O}_7$, a high-temperature superconductor under pressure, is key for unveiling the origin of its superconductivity. In this paper, we conduct a theoretical study of the electronic structure of the bilayer polymorph of $\text{La}_3\text{Ni}_2\text{O}_7$ using the hybrid functional approach, which is well suited to tackle the non-local correlation effects arising in this system from the molecular orbital splitting of the Ni $3d_{3z^2-r^2}$ states inside Ni-Ni dimers. Our calculations reveal that bilayer $\text{La}_3\text{Ni}_2\text{O}_7$ is a strongly correlated magnetic system with robust Ni spin moments. Spin moments on individual Ni sites take on unusually small values because of the electron delocalization over molecular orbitals involving multiple Ni and O sites. We further find that the magnetism of bilayer $\text{La}_3\text{Ni}_2\text{O}_7$ is intimately linked with charge distribution between different Ni and O orbitals. Two distinct regimes are identified in this regard. In one, molecular orbital physics drives the Ni $3d_{x^2-y^2}$ band towards half-filling, which is a well-established condition for unconventional high-temperature superconductivity upon hole doping in cuprates. In the other, the Ni $3d_{x^2-y^2}$ band is quarter-filled favouring spin- and charge-density wave states and Ni-O bond-disproportionation, which is consistent with several recent experimental claims. It is possible that superconductivity in $\text{La}_3\text{Ni}_2\text{O}_7$ occurs as a result of a pressure-induced transition between these two competing regimes. Since none of the low energy phases discovered in this study are metallic, non-stoichiometry would be required for superconductivity to occur.

PACS numbers:

I. INTRODUCTION

Unconventional Ni-based superconductivity continues to spark intense scientific interest, now reignited by the recent observation of a superconducting state up to 80 K in pressurized $\text{La}_3\text{Ni}_2\text{O}_7$ ¹⁻³. In distinction from the pioneering infinite-layer (IL) nickelate superconductors⁴, $\text{La}_3\text{Ni}_2\text{O}_7$ has a multilayer crystal structure featuring apical oxygen atoms between the NiO_2 planes in a multilayer and a high formal Ni oxidation state of 2.5+. The origin of superconductivity in $\text{La}_3\text{Ni}_2\text{O}_7$ is currently highly debated⁵⁻²⁹ and has become obscured even further by this material's recently discovered structural polymorphism³⁰⁻³². The focus of the present study will be on the bilayer variant of $\text{La}_3\text{Ni}_2\text{O}_7$, with double NiO_2 layers as shown in Fig. 1, which is particularly interesting due to claims of unique electronic features originating from the molecular orbital (MO) splitting of the Ni $3d_{3z^2-r^2}$ states within the Ni-Ni dimers⁸.

Advancing the understanding of $\text{La}_3\text{Ni}_2\text{O}_7$ requires an accurate knowledge of local charge distribution within the NiO_2 multilayers, especially in view of potential similarities with the cuprates and/or IL nickelates. In this regard, recent x-ray absorption spectroscopy³³ and electron energy loss spectroscopy³⁴ experiments on the bilayer $\text{La}_3\text{Ni}_2\text{O}_7$ have confirmed significant presence of oxygen holes in this system. This is what one typically finds in high-valence nickelates^{35,36}, such as the cubic $R\text{NiO}_3$ (R =rare-earth atom), as well as in hole doped cuprates. In these materials, the excess positive charge

beyond a valence of 2+ for Ni or Cu most likely resides as a hole in the O $2p$ valence states, although strongly hybridized with the transition metal $3d$ states. For the bilayer $\text{La}_3\text{Ni}_2\text{O}_7$, however, a detailed distribution of holes between the three different types of oxygen atoms (planar “O^p”, inner apical “O^a”, and outer apical “O^o”, see Fig. 1) remains to be explored. Since different locations and local symmetries of oxygen hole states are intimately linked with distinct Ni e_g orbital occupancies, such information is key for unveiling the microscopic mechanisms of superconductivity in $\text{La}_3\text{Ni}_2\text{O}_7$ and, more fundamentally, its electronic and magnetic ground state structure. For instance, holes in the planar O^p $2p_x$ and $2p_y$ orbitals are expected to form Zhang-Rice (ZR) singlets with local $x^2 - y^2$ symmetries or 3-spin polarons (3SP), which are hallmark features of cuprate-like superconductivity³⁷⁻³⁹.

The problem of the local oxygen hole density distribution in bilayer $\text{La}_3\text{Ni}_2\text{O}_7$ has been addressed theoretically by several first principles studies^{6,21,40-53} that offered many valuable insights but no consensus, nonetheless. A major theoretical challenge is to properly describe strong correlations between the Ni $3d$ electrons, which necessitates the use of density functional theory (DFT) methods that go beyond the local density approximation (LDA)⁵⁴. Methods like DFT+U^{55,56} or DFT+DMFT (dynamical mean-field theory)⁵⁷ are often considered a reasonable choice, but their accuracy is limited due to ambiguities regarding the double-counting correction, definition of correlated orbitals, and values of on-site interaction parameters. These limitations are known to be critical

for many strongly correlated systems, including the IL nickelates⁵⁸. Moreover, the characteristic MO splitting of the Ni $3d_{3z^2-r^2}$ states within the Ni-Ni dimers of a bilayer presents an additional complication in band theory as it signifies strong *non-local* correlation effects. A proper description of the latter requires the use of elaborate extended schemes in DFT+DMFT⁵⁰ and is beyond the applicability of DFT+U⁵⁹. It is also not possible within any type of band theory to define a local spin with eigenvalues of $S^2 = S(S+1)$. Model cluster approaches allow to avoid many of these issues, with a recent example coming from the cluster exact diagonalization study by Jiang *et al.*⁶⁰. Of course, the serious drawback of the latter approaches is the loss of translational symmetry.

In this paper, motivated to investigate bilayer $\text{La}_3\text{Ni}_2\text{O}_7$ from an unbiased *ab initio* standpoint, we choose to employ a hybrid functional approach⁶¹. It mitigates the self-interaction error by admixing a portion of exact exchange from Hartree-Fock (HF) theory into the DFT exchange-correlation energy. As such, this approach is free from the artificial dependencies on the double-counting correction scheme and the choice of correlated orbitals, with only adjustable parameters being the HF/DFT mixing parameter and (in certain cases) the interaction range. Within our hybrid functional approach, we find that the oxygen hole distribution in bilayer $\text{La}_3\text{Ni}_2\text{O}_7$ varies strongly depending on the type of imposed magnetic order. Some magnetic solutions are found to be metals, others are insulators or small band gap semiconductors. Some form spin- and charge-density-wave (SDW/CDW) states, which seem to be con-

nected to those observed in transport⁶², ^{139}La -nuclear magnetic resonance (NMR)^{63,64}, RIXS³³, neutron powder diffraction (NPD) and muon-spin rotation/relaxation (μSR) studies⁷¹.

The result is a very rich landscape of strongly differing electronic structures for the various possible spin orderings.

The structure of the paper is as follows. In Sec. II, we will provide computational details of our hybrid functional approach. In Sec. III, we will first review the non-magnetic electronic structure of bilayer $\text{La}_3\text{Ni}_2\text{O}_7$ and point out the differences in comparison with the previously published LDA results. Then, after discussing possible correlated local configurations in the light of the exact cluster diagonalization findings⁶⁰, we will present a selection of magnetically polarized and ordered states of bilayer $\text{La}_3\text{Ni}_2\text{O}_7$ and demonstrate significant variations in oxygen hole distribution patterns among them. We will also use hybrid functional based structural relaxation in order to explore the system's tendencies towards symmetry-breaking bond disproportionation and show that it might be hard to detect it using standard experimental structure characterization techniques. Finally, conclusions will be offered in Sec. IV.

II. METHODS

Our DFT calculations are performed using the pseudopotential code VASP⁶⁵ and the Heyd-Scuseria-Ernzerhof (HSE06) exchange-correlation hybrid functional⁶⁶. When not specified otherwise, the presented electronic structure results are obtained by setting the space group and the lattice constants of bilayer $\text{La}_3\text{Ni}_2\text{O}_7$ to those determined at a temperature of 300 K and an elevated pressure of 29.5 GPa (space group: $Fmmm$, $a = 5.289$, $b = 5.218$, $c = 19.734$ Å) and relaxing atomic positions within the gradient-corrected LDA⁶⁷. We use a $4 \times 4 \times 4$ Γ -centered \mathbf{k} -mesh for Brillouin zone integration in $\text{La}_3\text{Ni}_2\text{O}_7$ supercells containing two Ni-Ni dimers. As was confirmed in separate DFT+U calculations, this provides sufficiently well converged total energies and electronic states. The energy cut-off is set to ENCUT=320 eV.

III. RESULTS AND DISCUSSION

A. Non-magnetic electronic structure from HSE06: stabilization of the molecular orbital splitting

Let us first review key atomic orbitals and hybridization interactions that shape the electronic structure of bilayer $\text{La}_3\text{Ni}_2\text{O}_7$. These are well exposed in Figure 2, showing orbital projected electronic states of $\text{La}_3\text{Ni}_2\text{O}_7$ from a non-magnetic HSE06 calculation. This HSE06 result (also previously reported in Ref. 51) is qualitatively

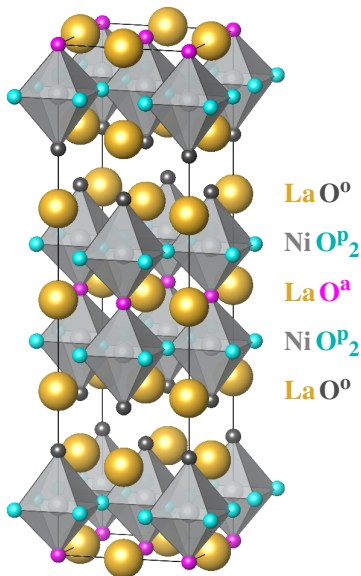


FIG. 1: The $Fmmm$ unit cell of bilayer $\text{La}_3\text{Ni}_2\text{O}_7$, where small balls of different colors indicate positions of the three types of oxygen atoms: planar (“O^P”), inner apical (“O^a”), and outer apical (“O^o”).

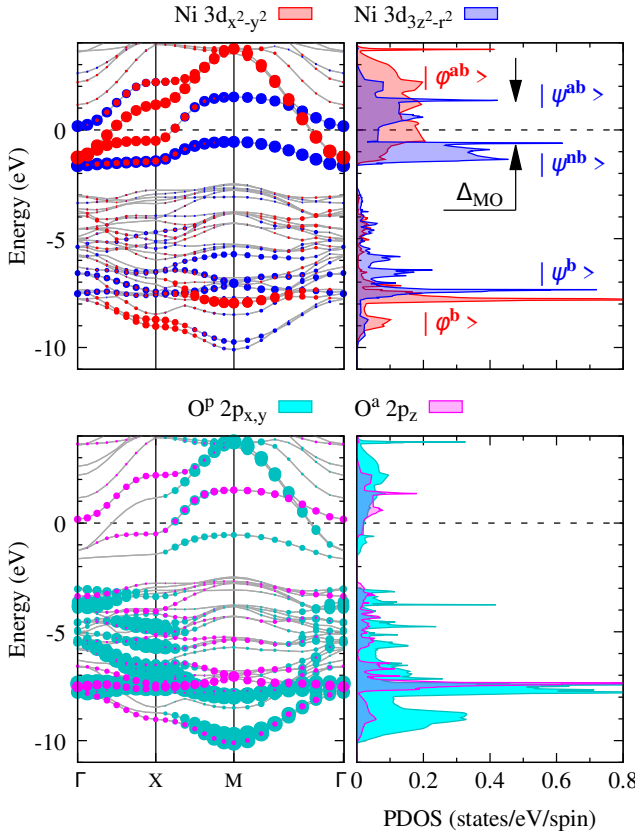


FIG. 2: Non-magnetic electronic structure of bilayer $\text{La}_3\text{Ni}_2\text{O}_7$ calculated with HSE06. The top (bottom) panels display projections onto the $\text{Ni } e_g$ ($\text{O } 2p$) orbitals, highlighting the MO splittings discussed in the main text. The splitting between the molecular $|\psi^{\text{nb}}\rangle$ and $|\psi^{\text{ab}}\rangle$ states, Δ_{MO} , is indicated by arrows.

similar with the LDA one¹, apart from the increased Ni-O states' bandwidth (from about 11 eV to 14 eV). Within both approximations, electronic structure near the Fermi level is dominated by $\text{Ni } e_g$ orbitals. The $\text{Ni } 3d_{x^2-y^2}$ orbitals are strongly hybridized with the planar oxygen $\text{O}^{\text{P}} 2p_x$ and $2p_y$ orbitals lying in the same NiO_2 plane via the hopping integral t_p , as shown in Figs. 3 (a, b). As a result, two MO *band* states (per plane) are formed:

$$\begin{aligned} & |\phi^{\text{b}}(\mathbf{k})\rangle = \alpha(\mathbf{k})|d_{x^2-y^2}\rangle \\ & \text{(bonding)} \quad + \beta(\mathbf{k}) \left(\sum_{i=1}^4 \eta_i(\mathbf{k}) |p_{\sigma}\rangle_i \right) \end{aligned}$$

and

$$\begin{aligned} & |\phi^{\text{ab}}(\mathbf{k})\rangle = \beta(\mathbf{k})|d_{x^2-y^2}\rangle \\ & \text{(anti-bonding)} \quad - \alpha(\mathbf{k}) \left(\sum_{i=1}^4 \eta_i(\mathbf{k}) |p_{\sigma}\rangle_i \right), \end{aligned}$$

where the subscripts $i = 1, 2, 3, 4$ run over the four corners of the oxygen square around a central $\text{Ni } 3d_{x^2-y^2}$

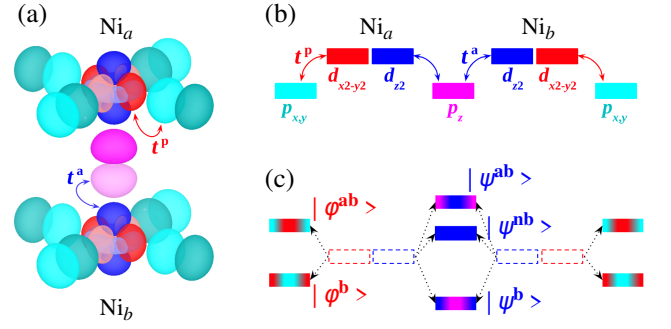


FIG. 3: A molecular orbital description of the $\text{La}_3\text{Ni}_2\text{O}_7$ electronic structure. (a) $\text{Ni } e_g$ and relevant $\text{O } 2p$ orbitals in a Ni-Ni dimer together with the t^{p} and t^{a} hopping integrals. (b) Energy levels of the $\text{Ni } e_g$ orbitals on Ni_a and Ni_b as well as of the inner apical $\text{O}^{\text{a}} 2p_z$ and planar $\text{O}^{\text{P}} 2p_{x,y}$ orbitals in the Ni-Ni dimer. (c) Energy levels of the MO states resulting from Ni-O hybridization.

orbital, $|p_{\sigma}\rangle_i$ are the p_x and p_y states centered at those corners that are σ -bonded to the central $\text{Ni } 3d_{x^2-y^2}$ orbital, and $\eta_i(\mathbf{k})$ are the symmetry respecting phases of individual oxygen atomic orbitals in the arising oxygen MO. This splitting is illustrated in Fig. 3 (c). The anti-bonding MO band crosses the Fermi level in a way similar to what is observed in the cuprates, apart from the fact that here this band is quarter-filled. Note that the normalizing coefficients $\alpha(\mathbf{k})$ and $\beta(\mathbf{k})$ are strongly \mathbf{k} -vector dependent, yielding no mixing at $\Gamma = (0, 0)$ ($\alpha = 0$ and $\beta = 1$) and maximum mixing at $M = (\pi, \pi)$ ($\alpha^2 \approx \beta^2 \approx 0.5$). Here, Γ and M are defined for the extended Brillouin zone of a single Ni-Ni dimer unit cell in the $Fm\bar{3}m$ structure.

In their turn, the $3d_{3z^2-r^2}$ orbitals of the two Ni atoms in a dimer [labeled as Ni_a and Ni_b in Figs. 3 (a, b)] each hybridize nearly as strongly with the $2p_z$ orbital of the central apical oxygen atom O^{a} via the hopping integral t_a . This gives rise to the following three MO states:

$$\text{(bonding)} \quad |\psi^{\text{b}}\rangle = \gamma(|d_{z^2}\rangle_a - |d_{z^2}\rangle_b) + \delta|p_z\rangle,$$

at around -8 eV,

$$\text{(non-bonding)} \quad |\psi^{\text{nb}}\rangle = (|d_{z^2}\rangle_a + |d_{z^2}\rangle_b)/\sqrt{2},$$

at -1 eV, and

$$\text{(anti-bonding)} \quad |\psi^{\text{ab}}\rangle = \delta(|d_{z^2}\rangle_a - |d_{z^2}\rangle_b) - \gamma|p_z\rangle,$$

at 1 eV. The “a” and “b” subscripts here refer to the two Ni atoms in the dimer. Effects due to $\text{Ni } 3d_{3z^2-r^2}$ hybridizing with the $\text{O}^{\text{P}} 2p_{x,y}$ combinations of the $x^2 + y^2$ symmetry are also present but weaker, since $3z^2 - r^2 = 2z^2 - (x^2 + y^2)$ and this results in the weaker dispersion in the xy plane. Note that, unlike $\alpha(\mathbf{k})$ and $\beta(\mathbf{k})$, the normalizing coefficients γ and δ are essentially independent of the \mathbf{k} -vector, irrespective of whether it is an in-plane

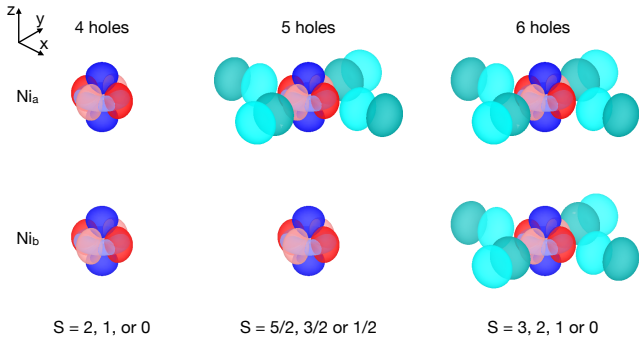


FIG. 4: An artist’s concept of the lowest energy hole distributions in Ni dimers. Possible spin states are indicated at the bottom. Left dimer has 4 holes occupying $3z^2 - r^2$ and $x^2 - y^2$ Ni $3d$ orbitals. Middle dimer has one extra hole in a linear combination of Oxygen p_x and p_y orbitals centred about one Ni with $x^2 - y^2$ symmetry. Both Ni ions have ligand holes associated with them as shown on the right for a 6 hole configuration.

and an out-of-plane one. In agreement with Ref. 51, we find that HSE06 corrects the underestimation of the bilayer coupling in LDA by increasing the energy separation between states $|\psi^{\text{nb}}\rangle$ and $|\psi^{\text{ab}}\rangle$, Δ_{MO} , from 1.5 to 2 eV. We would also like to note that the non-bonding state $|\psi^{\text{nb}}\rangle$ has no O^a $2p_z$ component because of an opposite parity between $|d_{z^2}\rangle_a + |d_{z^2}\rangle_b$ and $|p_z\rangle$. We will use this observation later to analyze magnetically polarized electronic structure of bilayer $\text{La}_3\text{Ni}_2\text{O}_7$.

Before concluding this section, we point out that oxygen orbitals other than O^p $2p_{x,y}$ and O^a $2p_z$ do not appear to play any significant role in the physics of bilayer $\text{La}_3\text{Ni}_2\text{O}_7$, including the outer apical oxygen O^o $2p$ orbitals, primarily because of their large spatial separation (> 2.20 Å) from the nearest Ni e_g orbitals.

B. Hole distribution configurations for a Ni-Ni dimer

While non-magnetic band structure from either LDA or HSE06 is helpful in identifying key orbitals and hybridization interactions, local electronic correlations and magnetism may affect orbital occupations dramatically. In this regard, let us review the *lowest-energy* hole distribution configurations within dimers containing four, five, and six holes, which are shown in Fig. 4. According to exact diagonalization calculations of Jiang *et al.*⁶⁰, these are all configurations with no hole in O^a $2p_z$. We continue to label Ni atoms within the same dimer as “a” and “b”, while two nearest-neighbour dimers are labelled as “A” and “B”. There are five holes per dimer in bilayer $\text{La}_3\text{Ni}_2\text{O}_7$ on average. They can get ordered as $A(a^3b^2)B(a^2b^3)$, which corresponds to a quarter filled band in both NiO_2 planes, but 5 holes on each dimer staggered on a and b . Also possible is configuration

$A(a^3b^3)B(a^2b^2)$, corresponding to alternation of 6 and 4 hole dimers, which can be achieved by transferring one hole from A to B , *i. e.*, a minimal charge fluctuation.

Let us now look at the spins. All the three-hole states involve a ZR singlet whose exchange interaction dominates strongly over the Hund’s rule exchange, leaving an $s = 1/2$ in the $d_{3z^2-r^2}$ orbital. All the two-hole cases are d^8 and with a spin of 1 (Hund’s rule exchange). Therefore, the spin on dimer $A(a^3b^2)$ is $a_{s=1/2}b_{s=1}$, and on $B(a^2b^3)$ it is $a_{s=1}b_{s=1/2}$. The intradimer exchange involving the $3z^2 - r^2$ orbitals on each a and b sites is antiferromagnetic and a result of superexchange between the two Ni via O^a of about 50 meV. This favours the dimer spin-1/2 state. Band theory, in which spin is not a good quantum number, would see this as $A(a_{s_z=+1/2}, b_{s_z=-1})$ and $B(a_{s_z=+1}, b_{s_z=-1/2})$ for a ferromagnetic in-plane coupling, and reversed signs for B for an antiferromagnetic coupling.

Now, we can also have the case of the alternating 6-hole - 4-hole dimers, $A(a^3, b^3)B(a^2, b^2)$, in which the ZR singlets would have $s = 0$, leaving the $3z^2 - r^2$ orbital with spin 1/2. The exchange interactions in this configuration would prefer a spin zero state for dimer A and spin 0 or 1 state for dimer B , which are closely spaced. However, DFT, which has only S_z projections, will see $A(a_{s_z=+1/2}, b_{s_z=-1/2})$ and $B(a_{s_z=+1}, b_{s_z=-1})$, or signs reversed for an antiferromagnetic in-plane coupling. This discussion illustrates that the results of exact diagonalization go generally beyond single particle band theories, unless there is a strong long-range magnetic order, in-plane and between planes.

For the less energetically favourable case of the fifth hole being located in the O^a $2p_z$ orbital [see Fig. 7 (b)], the inter-plane coupling would be ferromagnetic because this O hole and the two $3z^2 - r^2$ orbitals would want to form a 3-spin polaron³⁹ with the Ni spins parallel. As we will demonstrate later, an interesting feature of this configuration is that it preserves the MO splitting between the $|\psi^{\text{nb}}\rangle$ and $|\psi^{\text{ab}}\rangle$ states. However, mirroring the exact diagonalization findings, hybrid functional calculations find this configuration at a relatively higher energy, even with no quantum spin fluctuations taken into account.

C. Magnetically polarized HSE06 solutions and their distinct oxygen hole distribution patterns

As discussed above, strong electronic correlations in bilayer $\text{La}_3\text{Ni}_2\text{O}_7$ should give rise to localized magnetic moments on its Ni ions. Indeed, we find in our hybrid functional calculations that a magnetically polarized state with a finite magnetic moment on Ni is by at least 0.75 eV per Ni lower in energy compared with a non-magnetic one, irrespective of the type of magnetic ordering. It is noteworthy that most of this per Ni energy lowering is a result of the Hund’s exchange between the Ni $3d_{3z^2-r^2}$ and $3d_{x^2-y^2}$ orbitals with spin parallel elec-

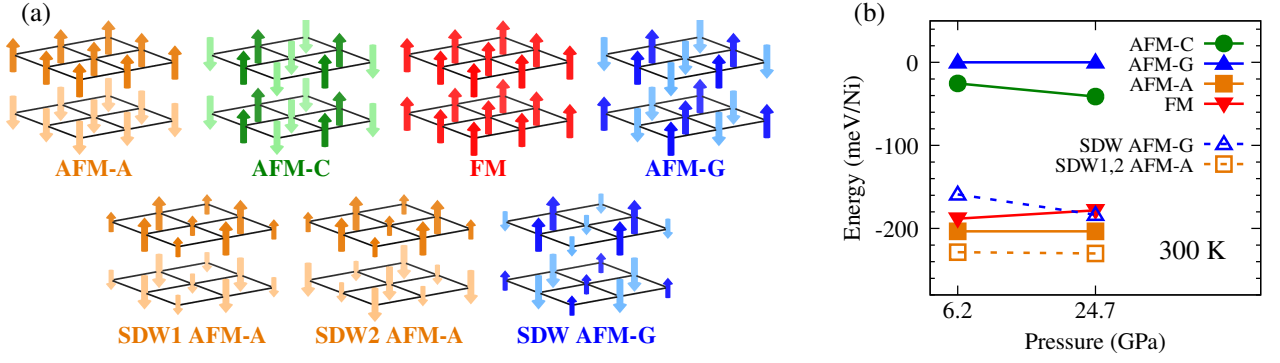


FIG. 5: (a) Magnetic configurations of bilayer $\text{La}_3\text{Ni}_2\text{O}_7$ considered in the main text and (b) their relative total energies per Ni calculated in HSE06 using low- and high-pressure structural parameters. In (a), arrows represent the orientations of Ni spin magnetic moments at different sites of the bilayer square lattice.

tron occupations. This Hund's rule exchange for Ni^{2+} in the d^8 configuration is about 0.65 eV taking into account the substantial degree of covalence which dilutes the effects of the atomic exchange and correlations from that of purely ionic materials. Several recent experiments confirm presence of localized magnetic moments in $\text{La}_3\text{Ni}_2\text{O}_7$, including RIXS³³ and muon spin relaxation⁶⁸.

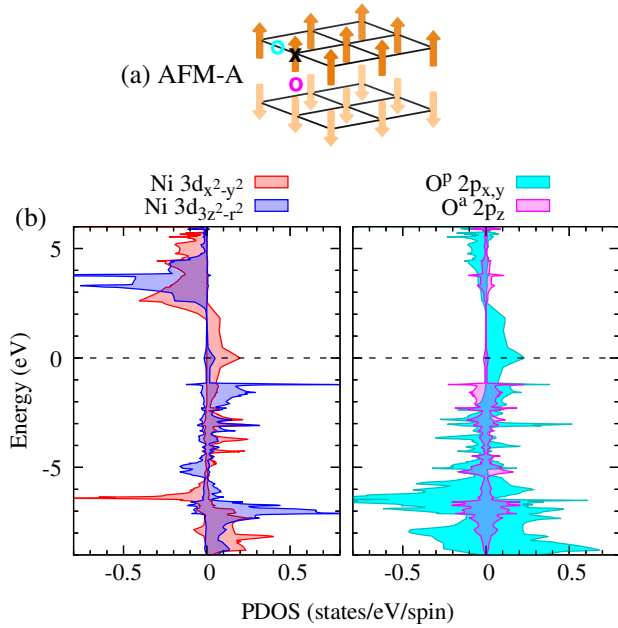


FIG. 6: HSE06 electronic structure of the uniform AFM-A phase in bilayer $\text{La}_3\text{Ni}_2\text{O}_7$: (a) the AFM-A magnetic configuration and (b) the spin-resolved projected densities of states (PDOSs) for the Ni e_g orbitals (left panel) and selected O $2p$ orbitals (right panel) with multiplicity factors taken into account. Here in (a) and also in the subsequent similar figures, the “x” and “o” symbols indicate the Ni or O atoms for which the PDOSs in (b) were generated for.

DFT is a method that only allows to explore microscopic states in which magnetic moments are statically ordered. Therefore, in the following we will consider magnetically ordered $\text{La}_3\text{Ni}_2\text{O}_7$ configurations, as computationally accessible proxies to its true, strongly fluctuating, magnetic ground state. Besides, some experiments claim $\text{La}_3\text{Ni}_2\text{O}_7$ to be close to developing a long-range magnetically ordered state^{33,62,68}. Figure 5 (a) displays the seven Ni spin configurations considered in this work, while their relative energies at different pressure values can be found in Fig. 5 (b) and their energy gaps and Ni magnetic moments in Table I. These configurations include a ferromagnetic (FM) one, three antiferromagnetic ones (AFM-G, AFM-C, AFM-A) and three SDW ones (SDW AFM-G, SDW1 AFM-A, SDW2 AFM-A). The AFM-A and FM configurations, both characterized by an FM in-plane spin ordering, are among the lowest energy states in HSE06, which is in qualitative agreement with DFT+U calculations of Geisler *et al.*⁴⁸. This ferromagnetic coupling is the result of the coupling of an O^p $2p_{x,y}$ hole in the bridging position between two Ni's with spin 1 and can also be described in terms a 3- (or in this case actually 5-) spin polaron with a lowest energy state of total spin 3/2 rather than the spin 1/2 in the cuprates³⁹. 3SP is an alternative description of the influence of the O $2p$ holes to the Zang-Rice singlet like description of the cuprates involving only one central cation. Curiously, we find that the AFM-A configuration, along with the AFM-G one, is unstable towards the formation of SDW states whereby Ni magnetic moments on different lattice sites disproportionate in magnitude, as indicated in Fig. 5 (a) by arrows of different sizes. There are two nearly degenerate SDW/CDW states associated with the AFM-A configuration. As will be explained below, this is accompanied by charge-density waves of corresponding symmetries. All SDW/CDW phases are found to have lower energies than their uniform counterparts.

We first focus attention on the uniform moment solutions. The lowest energy uniform solution is AFM-A, with ferromagnetic planes coupled antiferromagnetically.

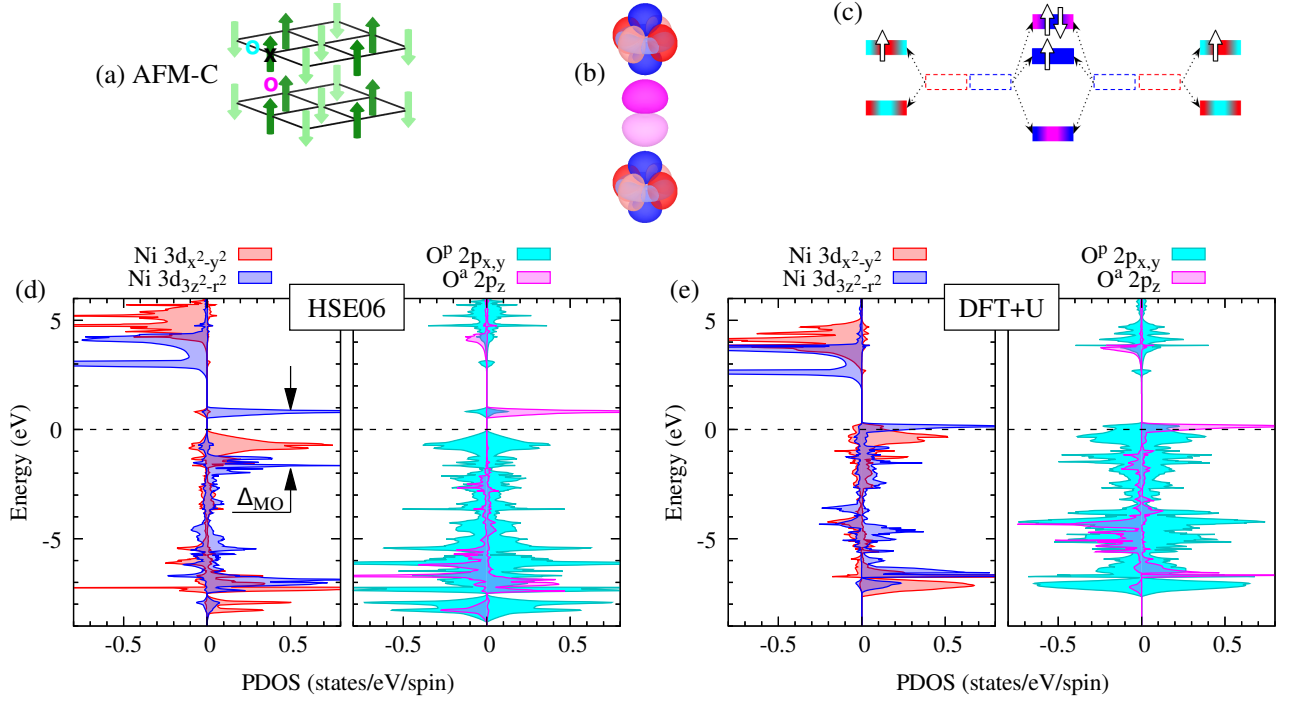


FIG. 7: Electronic structure of the AFM-C magnetic phase in bilayer $\text{La}_3\text{Ni}_2\text{O}_7$: (a) the AFM-C magnetic configuration, (b) the Ni-Ni dimer with a hole in $\text{O}^a 2p_z$ (c) schematic distribution of the five holes (up and down arrows) between the MO states in a Ni-Ni dimer, (d) HSE06 spin-resolved PDOS for the e_g orbitals of one Ni in the dimer (left panel) and for the apical $\text{O} 2p_z$ and planar $\text{O} 2p_{x,y}$ orbitals (right panel), with multiplicity factors taken into account, (e) same as (d) but obtained within DFT+U. In (d), the splitting between the molecular states $|\psi^{\text{nb}}\rangle$ and $|\psi^{\text{ab}}\rangle$, Δ_{MO} , is indicated by arrows.

We have pointed out that the 3SP model rather than the ZR singlet model directly provides a ferromagnetic coupling between the two Ni. So, for this configuration the holes must be on O^p . This naturally leaves the closed shell O^a providing the antiferromagnetic exchange between the Ni spins in a dimer. This is consistent with the oxygen PDOS in Fig. 6, where $\text{O}^a 2p_z$ is all but fully occupied with equal amounts of spin up and spin down. It is interesting to note that this magnetic configuration

TABLE I: HSE06 energy gaps and Ni magnetic moments of the considered magnetic configurations in bilayer $\text{La}_3\text{Ni}_2\text{O}_7$.

	Gap (eV)	μ (μ_B)
FM	0.00	1.40
AFM-C	0.52	1.25
AFM-G	0.00	1.09
AFM-A	0.00	1.32
SDW AFM-G	1.22	1.50/0.41
SDW1 AFM-A	0.77	1.47/1.13
SDW2 AFM-A	0.71	1.45/1.14

produces an electronic state in which the upper plane states above the Fermi energy, E_F , are almost solely spin up while the lower plane states are almost solely spin down, corresponding to two half-metallic ferromagnetic planes with opposite spin. We should note also that the hole density of states just above E_F has an almost equal amount of $\text{Ni } 3d_{x^2-y^2}$ and $\text{O}^p 2p_{x,y}$ orbital characters, consistent with a very strong hybridization between them and consistent with the 3SP picture discussed above resulting in a ferromagnetic in-plane coupling. Indeed, there is enough $\text{O}^p 2p_{x,y}$ hole density in the planes to result in a ferromagnetic in-plane coupling via an oxygen hole between the two spins 1 on neighbouring in-plane Ni sites, which each couple with the spin of the common oxygen hole into a net spin-3/2 state. In DFT, this will result in Ni z -axis projected magnetic moments that are equal, sharing this S_z projection of $S = 3/2$, *i. e.*, a local z projected moment of about $1.5 \mu_B$. This is reduced to $1.32 \mu_B$ by the covalent hybridization with oxygen, as one can see in Table I.

Now, let us compare this configuration with the PDOS of the less energetically favourable AFM-C phase in Fig. 7 (c), where the planes are in a G-type antiferromagnetic arrangement with inter-plane Ni dimer coupling being ferromagnetic. The electronic structure has changed dramatically! The material is now a 1 eV gap semicon-

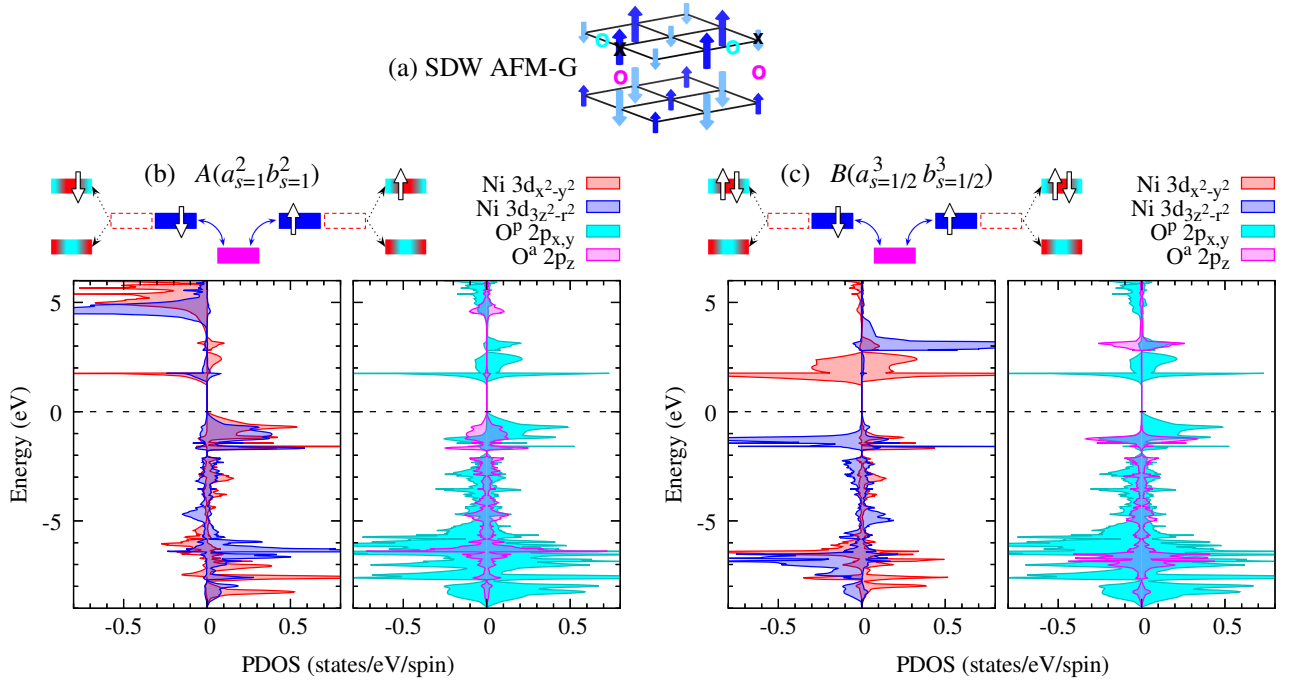


FIG. 8: HSE06 electronic structure of the SDW AFM-G phase in bilayer $\text{La}_3\text{Ni}_2\text{O}_7$: (a) the SDW AFM-G magnetic configuration, with a checkerboard order of large and small Ni spin dimers, (b,c) schematic distributions of holes and PDOS for the (b) large and (c) small spin Ni dimers. In (a), the three colored “x” and “o” symbols on the left pertain to the PDOSs shown in (b) and those three on the right to the PDOSs in (c).

ductor with the oxygen hole density just above E_F occupying the inter-plane oxygen O^a . These empty $\text{O}^a 2p_z$ states form an extremely narrow band because of the small inter-dimer electron hopping between the $\text{O}^a 2p_z$ as well as $\text{Ni } 3d_{3z^2-r^2}$ orbitals. In AFM-A, the ferromagnetic coupling was provided by the holes being in the in-plane O^p while now, with holes in the inter-plane O^a , the double exchange occurs between the $\text{Ni } 3d_{3z^2-r^2}$ orbitals and is ferromagnetic. For this configuration, the Ni_2O_9 cluster eigenstates resemble closely those of a 3SP, as shown by Jiang *et al.*⁶⁰, while the band theory approach replaces this with spin polarization of molecular orbital states $|\psi^{\text{nb}}\rangle$ and $|\psi^{\text{ab}}\rangle$, as illustrated in Fig. 7 (b). An intriguing consequence of this oxygen hole density redistribution is that the anti-bonding $x^2 - y^2$ -symmetry MO band $|\phi^{\text{ab}}(\mathbf{k})\rangle$ is now half-filled, whereas it was quarter-filled in the AFM-A phase. The spin-polarized molecular orbitals in band theory are created to describe the anti-ferromagnetic internal exchange between the $\text{O } 2p_z$ and each of the $\text{Ni } 3d_{3z^2-r^2}$ orbitals. In the cluster exact diagonalization, on the other hand, this is described in terms of a net cluster lowest-energy total spin of $3/2$, leaving the S_z degeneracy open for inter-cluster interactions. In DFT, each Ni’s individual spin projections s_z will equally share this total S_z minus the now substantial spin on O^a leading to an s_z projection on each Ni of considerably less than $1.5 \mu_B$, as seen in Table I.

Before going onto the other phases, we have also shown

in Fig. 7 a comparison of the HSE06 and LDA+U calculations for the AFM-C phase. Here, we use the following parameters for the DFT+U method: $U = 6$ and $J_H = 0.7$ eV for $\text{Ni } 3d$ electrons and $U = 6$ eV for $\text{La } 4f$ electrons^{55,56,69}. We see that the PDOS between the two methods are closely related showing very little resemblance to the non-magnetic solution. One also sees that, while qualitatively capturing the energy splitting between the $x^2 - y^2$ symmetry states and between the empty minority spin MO states, DFT+U fails to properly separate the empty majority spin MO states $|\psi^{\text{ab}}\rangle$ from the full majority spin MO states $|\psi^{\text{nb}}\rangle$ and, as a result, to open up an energy gap at the Fermi level. Interestingly, we can also use the comparison between the hybrid functional and DFT+U results to approximately deduce a realistic value for the $\text{Ni } 3d$ on-site Coulomb repulsion parameter U . It appears that even $U = 6$ eV is too low a value, albeit only slightly, to yield the 6 eV splitting between the empty and occupied $x^2 - y^2$ symmetry bands given by HSE06. This observation questions the choice for significantly lower U values of 3 or 3.5 eV that were employed in some of the previously published DFT+U studies of bilayer $\text{La}_3\text{Ni}_2\text{O}_7$ ^{48,49}.

We now look at the non-uniform moment SDW cases. These phases are generated by disproportionated magnetic moments from the AFM-G and AFM-A phases. Their PDOSs are shown in Figs. 8-10. These SDW phases are all at lower energies (by about 30 or 160 meV per Ni)

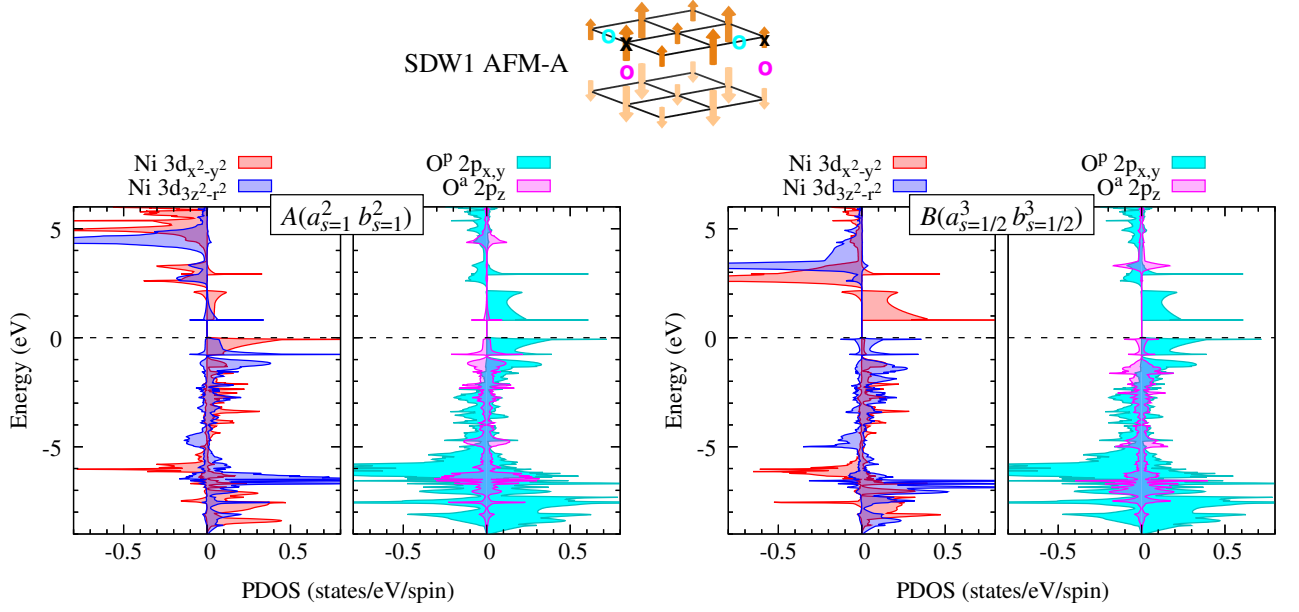


FIG. 9: HSE06 electronic structure of the SDW1 AFM-A phase in bilayer $\text{La}_3\text{Ni}_2\text{O}_7$: (a) the SDW1 AFM-A magnetic configuration, with a checkerboard order of large and small Ni spin dimers, (b,c) PDOSs for the (b) large and (c) small spin Ni dimers.

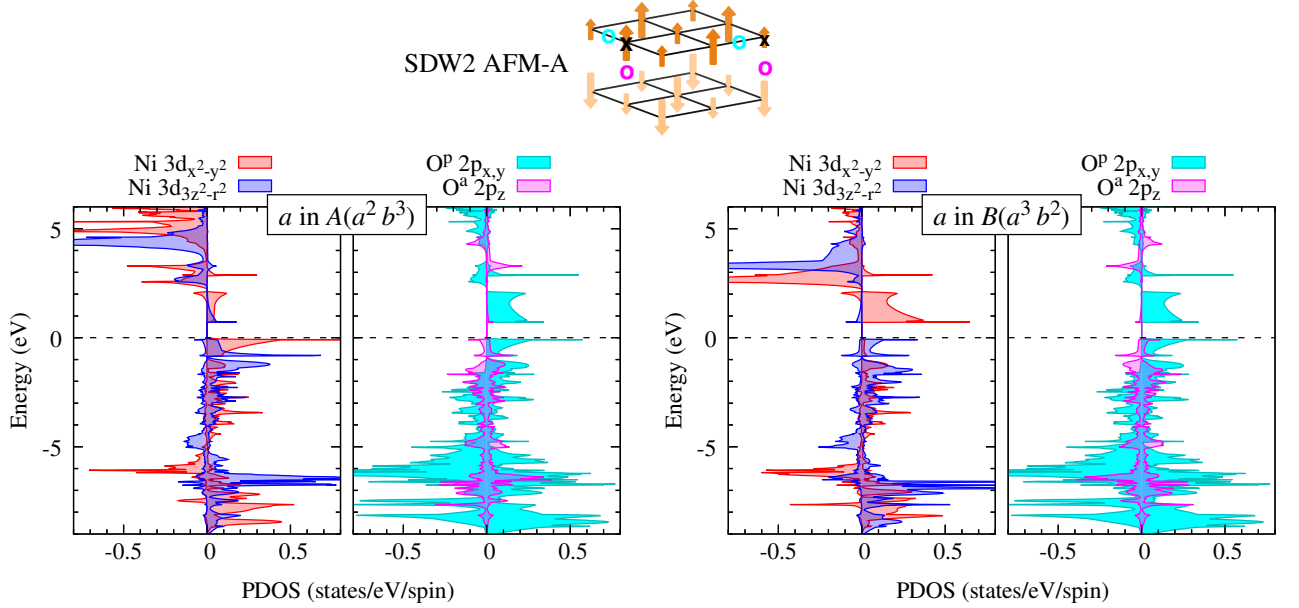


FIG. 10: HSE06 electronic structure of the SDW2 AFM-A phase in bilayer $\text{La}_3\text{Ni}_2\text{O}_7$: (a) the SDW2 AFM-A magnetic configuration, with a checkerboard order of large and small Ni spin sites in each plane and with a phase shift between the planes, (b,c) PDOSs for the (b) large and (c) small spin Ni sites.

than the parent phases, which is a considerably strong stabilization. They each represent a checkerboard pattern of large and small moments in each of the two planes. The AFM-G SDW phase has the same type of antiferromagnetic ordering both in the planes and between the planes with an in-phase checkerboard pattern of small

and large moments. The PDOS in Fig. 8 shows us a very large low-energy extra Ni $3d_{x^2-y^2}$ hole density with a strongly diminished in-plane $\text{O}^p 2p_{x,y}$ occupation. It also shows us a strong CDW accompanying the SDW. Going back to our notation of the charge ordering as between two dimers labelled by A and B and within each

dimer between two Ni's labelled as a and b , we would label this configuration as $A(a_{s=1}^2, b_{s=1}^2)B(a_{s=1/2}^3, b_{s=1/2}^3)$, *i. e.*, the four hole – six hole case. Interestingly, the large spin here has the smaller hole density, which means that to add holes but lower the spin we must be forming $s = 0$ states between pairs of spins. This can be done with either ZR singlets or doubly occupied Ni $3d_{x^2-y^2}$ states. Looking at the low-spin and large hole density dimer B [Fig. 8 (c)] just above E_F , it seems to be the d^7 state, with two holes in the Ni $3d_{x^2-y^2}$ orbitals and one in the Ni $3d_{3z^2-r^2}$ orbital, that causes the low spin, rather than the ZR singlet plus a Ni $3d_{3z^2-r^2}$ hole. We know from the cluster calculations that the d^7 $s = 1/2$ state is close in energy to the ZRS plus a Ni $3d_{3z^2-r^2}$ hole state also of spin $1/2$.

We now turn to the AFM-A SDW phases, of which there are two, with nearly the same energies (see Figs. 9 and 10). The AFM-A phase has ferromagnetic planes coupled antiferromagnetically. This is also the case in the two SDW phases, with also ferromagnetic planes coupled antiferromagnetically but with each having a checkerboard pattern of alternating high- and low-spin Ni magnetic moments. In SDW1, the spin size alternating patterns of the two planes are in phase, while in SDW2 they are in anti-phase. With regard to the hole occupations, the first one has the same four hole – six hole ordering as in SDW AFM-G, and the second one has the five – five, *i. e.*, $A(a_{s=1}^2, b_{s=1/2}^3)B(a_{s=1/2}^3, b_{s=1}^2)$, hole ordering. As one can see in Figs. 9 and 10, their PDOSs are rather similar, indicating that super exchange via the inter-planar O^a does not affect charge distribution much. Indeed, this super exchange interaction is only about 50 meV according to the cluster calculations while the ZRS exchange interaction between the ligand hole (\underline{L}) on O^p and the Ni $3d_{x^2-y^2}$ hole is very large between 1 and 2 eV. We also see from the PDOSs that the large-spin dimer again has little O^p $2p_{x,y}$ hole density, while the low-spin one has a lot but also a lot of Ni $3d_{x^2-y^2}$ low-energy hole density, similar to what we see in the AFM-A phase, which we designated as the result of a 3SP involving two Ni's and the in-between O^p rather than a ZR singlet, with now significant $p_{x,y}$ and $d_{x^2-y^2}$ densities of the same spin at low hole energies.

Making a connection with the real picture, one should keep in mind that all band-structure applications of DFT produce single-Slater-determinant single-particle states restricted by translational symmetry, which consider z -projections of spins to be good quantum numbers and not the spins themselves. This creates a real problem for states that are locally antiferromagnetically coupled. For example, spin-1/2 antiferromagnetically coupled states form singlets and triplets, with the singlets at the energy of $-\frac{3}{4}J$ and the triplets at $+\frac{1}{4}J$. However, if we assume Ising spins and consider only the S_z component, the energies are $-\frac{1}{4}J$ and $+\frac{1}{4}J$. So, the stabilization of singlet-like states with zero net spin is $-\frac{1}{2}J$ lower than that generated by assuming Ising spins. This means that all the states that potentially involve local singlets will in reality

be considerably lower in energy than the $S_z = 0$ states generated by band-structure methods, which should be distinguished from the $S = S_z = 0$ states of two identical orbitals being occupied by a spin-up and a spin-down electron because of the Pauli exclusion principle and not because of exchange. This is especially important if the number of neighbours a central spin is coupled to is small. Indeed, if it is smaller than three, then the singlet solution is generally much more stable than the S_z only spin ordered states. For bilayer $La_3Ni_2O_7$, this especially strongly influences the inter-plane or intra-cluster exchange between the Ni $3d_{3z^2-r^2}$ orbitals generated by the coupling to an O^a $2p_z$ hole, *i. e.*, the 3SP case. These states involve very strong quantum fluctuations resulting in a net spin that is delocalized over the cluster, which complicates the effective inter-cluster interactions and the global magnetic structure. In general, all states involving an O hole either in-plane or between planes that is strongly antiferromagnetically coupled to its nearest-neighbour Ni spins will in reality have considerably lower energies than what is predicted by band-structure methods.

Concluding this part we see a strong relationship between the charge density and the spin density and the type of coupling, be it ferromagnetic or antiferromagnetic, which strongly complicates the electronic and magnetic structure of the lowest-energy states. We see strong tendencies towards the formation of molecular orbitals if the O low-energy hole density is strong. If the fifth hole of the dimer is in the inter-planar position, we have a strong ferromagnetic coupling due to double exchange and the formation of a 3-spin polaron. If this O is fully occupied, which it is in all the low-energy cases, then the inter-planar exchange is antiferromagnetic, but, because of the low Ni-Ni coordination number of one, these $3z^2 - r^2$ orbitals will tend to form, via the intervening O, singlet states rather than to participate in an antiferromagnetic like spin structure. However, that will only happen if the much stronger Hund's rule exchange is strongly reduced because of the dilution effect resulting from a strong covalency. We reached the conclusion that the two nearly degenerate AFM-A SDW phases are the lowest-energy ones. It is interesting to note that in these lowest-energy phases the in-plane spin correlation is ferromagnetic. Of course, it is quite possible that for a larger supercell we could have a longer wave-length SDW/CDW, involving, for example, ferromagnetic pairs coupled antiferromagnetically.

D. Bond disproportionation in the SDW/CDW states

All of the considered SDW/CDW states are found to be further stabilized by Ni-O bond disproportionation, whereby alternating large and small oxygen squares are formed around the d^8 and $d^8 \underline{L}_{x^2-y^2}$ Ni sites, respectively. This also further favours the ZRS like states in

the small squares relative to the 3SP like description. Table II summarizes the relative total energies and Ni-O bond lengths of the AFM-C, AFM-G, SDW AFM-G, and SDW1 AFM-A states discussed above, but at $T = 300$ K and near-ambient $P = 1.6$ GPa. These results are obtained by performing full relaxation of atomic positions within HSE06. Full structural information on these four fully optimized structures can be found in the Appendix. Comparing Table II and Fig. 5 (b), one can see that allowing for bond disproportionation increases the energy separation between the uniform Néel and SDW/CDW states by about 100 meV per Ni.

Curiously, we find that even though the Ni-O bond disproportionation is quite significant and also reduces the structural symmetry of bilayer $\text{La}_3\text{Ni}_2\text{O}_7$ (for instance, from $Amam$ to $Amm2$ at $T = 300$ K and $P = 1.6$ GPa), this could be hard to detect with standard x-ray diffractometry. Figure 11 shows simulated diffraction patterns of the fully relaxed bilayer $\text{La}_3\text{Ni}_2\text{O}_7$ in the AFM-C and SDW AFM-G states at $T = 300$ K and $P = 1.6$ GPa. The simulations have been done using the VESTA code⁷⁰. The differences between the two diffractograms are barely detectable and might be beyond the experimental resolution. We therefore urge experimental groups to reexamine results of structural characterization of this nickelate in view of potential Ni-O bond disproportionation triggered by an onset of a SDW/CDW state.

IV. SUMMARY AND DISCUSSION

In summary, we studied the electronic properties of the bilayer polymorph of $\text{La}_3\text{Ni}_2\text{O}_7$, a high-temperature superconductor under pressure, using the unbiased hybrid functional approach. We found a strong tendency for this system to develop localized magnetic moments on Ni ions and explored a variety of its magnetically ordered configurations, comparing their energetics and the associated microscopic charge distribution patterns.

We summarize some of the most important findings.

TABLE II: Relative total energies and Ni-O distances in selected magnetic states of bilayer $\text{La}_3\text{Ni}_2\text{O}_7$ as obtained within HSE06 after full atomic position relaxation with the lattice parameters fixed to those measured experimentally at $T = 300$ K and $P = 1.6$ GPa.

	Energy (meV/Ni)	Ni-O ^a (Å)	Ni-O ^p (Å)	Ni-O ^o (Å)
AFM-C	-17	1.97	1.93	2.20
AFM-G	0	2.00	1.93	2.24
SDW AFM-G	-298	2.00/2.00	2.00/1.86	2.20/2.28
SDW1 AFM-A	-319	2.00/2.00	1.99/1.87	2.19/2.29

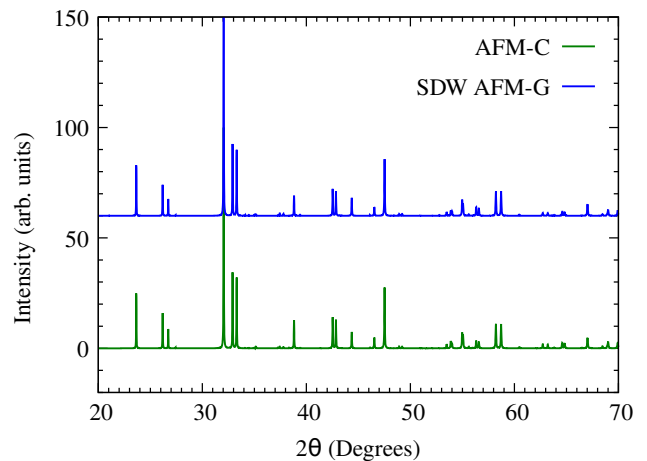


FIG. 11: X-ray diffractograms simulated for the high-symmetry AFM-C state and the symmetry-broken bond-disproportionated SDW AFM-G state, demonstrating barely noticeable differences.

First of all, the energy difference between the non-magnetic and magnetically ordered phases was found to be close to 0.75 eV per Ni, which corresponds to the Hund's rule coupling energy that appears with magnetic order but vanishes without magnetic order. Also of general importance is that all of the magnetic structures consistent with 4 Ni atoms per unit cell converged to energies in the range of 300 meV per Ni at most. What was really surprising to us is the exceptionally strong dependence of the low energy scale (*i. e.*, ± 1.5 eV around E_F) electronic structure on the type of magnetic order. Some magnetic structures were metallic, other semiconducting with gaps varying from about 0.5 to 1.2 eV. The z -projected magnetic moments varied between 1 and $1.5 \mu_B$, corresponding to a spin on Ni half way between $1/2$ and 1, which is half way between what is expected for Ni^{3+} ($S = 1/2$) and Ni^{2+} ($S = 1$) if we consider a hole in only the e_g symmetry crystal field split states.

Looking at the spin, orbital, and atomic projected densities of states, we conclude that the extra 0.5 holes per Ni beyond the base $\text{Ni}^{2+} d^8$ configuration mainly occupy the O $2p$ states of either in-plane $x^2 - y^2$ symmetry about a particular Ni or, in some extreme cases, the inter-planar O^a $2p_z$ orbitals. The latter was only found in those magnetic structures where the inter-planar spin coupling was ferromagnetic. These structures, however, also had considerably higher total energies than the magnetic structure with an antiferromagnetic inter-planar coupling. This is consistent with the exact diagonalization cluster calculations⁶⁰. We conclude that bilayer $\text{La}_3\text{Ni}_2\text{O}_7$ quite strongly prefers not to have hole occupation of the inter-planar O^a $2p_z$ orbitals in its lowest energy magnetic and charge density states.

Although Ni is expected to be $2.5+$ on average, we find that the the majority of the extra 0.5 missing electrons are located on the neighbouring O $2p$ orbitals forming

molecular orbital like states, which for the lowest total energy states correspond to holes in the NiO_2 planes in a $x^2 - y^2$ symmetry combination of O^p $2p_{x,y}$ nearest-neighbour orbitals relative to a central Ni's orbitals. These (in band theory) form molecular orbital states with the Ni $3d_{x^2-y^2}$ orbitals, involving also the Ni states with two holes in the $x^2 - y^2$ orbitals. In the exact diagonalization cluster calculations, these orbitals form Zhang-Rice singlet like states involving also the Ni low-spin d^7 states. This brings us close to the cuprates, aside from the fact that using the cuprate language this material would be 50% hole-doped (*i. e.*, in the extreme overdoped region) and in addition there still is the spin 1/2 remaining in the $3z^2 - r^2$ orbitals for those Ni's that are involved in ZR singlets.

If we ordered these spins and charges in a checkerboard fashion, we would have half of the Ni's involved in ZR singlets, with a remaining spin of 1/2 in a $3z^2 - r^2$ orbital, and the other half would be close to Ni^{2+} with a spin of 1. This explains the 3 different kinds of spin and charge density wave states found in our hybrid functional calculations. The lowest energy 2 such CDW/SDW phases are of the AFM-A type, *i. e.*, ferromagnetic planes ordered antiferromagnetically. Qualitatively, this is also what is found in the exact diagonalization study⁶⁰ and corresponds to the ZRS - Ni^{2+} checkerboard patterns in the two planes. These can be in phase, corresponding formally to the 6 hole - 4 hole cluster ordering, or out of phase, corresponding to the 5 hole - 5 hole ordering. This leads to the same kind of possible CDW/SDW structures that are found in the combined neutron powder diffraction (NPD) and muon-spin rotation/relaxation (μSR) study⁷¹. The total energy difference between these phases is very small of the order of 5 meV in hybrid functional calculations. However, we should note that, in spite of the energetic preference of the AFM-A CDW/SDW phases, the AFM-G SDW phase is the closest to the experimental magnetic moments in the

NPD/ μSR study. The theoretical spin disproportionation is quite small for the AFM-A SDW phase compared to experiment.

We also studied the relaxed CDW/SDW structures and found that there was a considerable breathing mode like bond disproportionation in the phases with the ZRS like states. The Ni-O distance in the short bond was reduced by about 0.1 Å, which is a very substantial bond disproportionation. Nonetheless, it is important that this bond disproportionation was all but invisible in the theoretical x-ray diffraction simulations. This kind of strong disproportionation is rather similar in size to that of BaBiO_3 , which suggests a very strong electron-phonon coupling.

V. APPENDIX

Tables III to VI present atomic positions of the four bilayer $\text{La}_3\text{Ni}_2\text{O}_7$ phases, AFM-C, AFM-G, SDW AFM-G, and SDW1 AFM-A, that were fully relaxed in HSE06 while keeping the lattice constants fixed to those measured experimentally at room temperature and low pressure of 1.6 GPa.

VI. ACKNOWLEDGMENTS

The authors would like to thank the Stewart Blusson Quantum Matter Institute and the Natural Sciences and Engineering Research Council of Canada for providing financial support and computational resources.

TABLE III: HSE06 relaxed atomic positions for the uniform AFM-C magnetic configuration.

AFM-C at 1.6 GPa, space group: $Cmcm$			
$a = 20.403$, $b = 5.3768$, $c = 5.4392$ Å, $\alpha = \beta = \gamma = 90^\circ$			
atom	x	y	z
Ni	0.0956	0.2470	0.25
La1	0.1785	0.2573	0.75
La2	0.5	0.2374	0.25
O1	0.0848	0.5	0.5
O2	0.0	0.1961	0.25
O3	0.1073	0.0	0.0
O4	0.2025	0.2908	0.25

TABLE IV: HSE06 relaxed atomic positions for the uniform AFM-G magnetic configuration.

AFM-G at 1.6 GPa, space group: $Cmcm$			
$a = 20.403$, $b = 5.3768$, $c = 5.4392$ Å, $\alpha = \beta = \gamma = 90^\circ$			
atom	x	y	z
Ni	0.0965	0.2460	0.25
La1	0.1806	0.2604	0.75
La2	0.5	0.2473	0.25
O1	0.0868	0.5	0.5
O2	0.0	0.1850	0.25
O3	0.1099	0.0	0.0
O4	0.2056	0.2945	0.25

TABLE V: HSE06 relaxed atomic positions for the bond-disproportionated SDW AFM-G magnetic configuration.

SDW AFM-G at 1.6 GPa, space group: $Amm2$			
$a = 5.4392, b = 20.403, c = 5.3768 \text{ \AA}, \alpha = \beta = \gamma = 90^\circ$			
atom	x	y	z
Ni1	0.5	0.9032	0.3961
Ni2	0.0	0.5963	0.4037
La1	0.0	0.8196	0.4070
La2	0.5	0.6806	0.3876
La3	0.5	0.5	0.4031
La4	0.0	0.0	0.4114
O1	0.2422	0.4140	0.1613
O2	0.5	0.0	0.3412
O3	0.0	0.5	0.4728
O4	0.7571	0.8897	0.1389
O5	0.5	0.7963	0.4403
O6	0.0	0.7070	0.3478

TABLE VI: HSE06 relaxed atomic positions for the bond-disproportionated SDW1 AFM-A magnetic configurations.

SDW1 AFM-A at 1.6 GPa, space group: $Amm2$			
$a = 5.4392, b = 20.403, c = 5.3768 \text{ \AA}, \alpha = \beta = \gamma = 90^\circ$			
atom	x	y	z
Ni1	0.5	0.9033	0.3962
Ni2	0.0	0.5961	0.4039
La1	0.0	0.8196	0.4071
La2	0.5	0.6807	0.3873
La3	0.5	0.5	0.4030
La4	0.0	0.0	0.4105
O1	0.2433	0.4138	0.1598
O2	0.5	0.0	0.3407
O3	0.0	0.5	0.4726
O4	0.7559	0.8898	0.1397
O5	0.5	0.7963	0.4394
O6	0.0	0.7072	0.3474

¹ H. Sun, M. Huo, X. Hu, J. Li, Z. Liu, Y. Han, L. Tang, Z. Mao, P. Yang, B. Wang, et al., Nature **621**, 493 (2023),

ISSN 1476-4687.

² J. Hou, P.-T. Yang, Z.-Y. Liu, J.-Y. Li, P.-F. Shan, L. Ma,

- G. Wang, N.-N. Wang, H.-Z. Guo, J.-P. Sun, et al., Chinese Physics Letters **40**, 117302 (2023), URL <https://dx.doi.org/10.1088/0256-307X/40/11/117302>.
- ³ Y. Zhang, D. Su, Y. Huang, Z. Shan, H. Sun, M. Huo, K. Ye, J. Zhang, Z. Yang, Y. Xu, et al., Nature Physics (2024), ISSN 1745-2481.
 - ⁴ D. Li, K. Lee, B. Y. Wang, M. Osada, S. Crossley, H. R. Lee, Y. Cui, Y. Hikita, and H. Y. Hwang, Nature **572**, 624 (2019), ISSN 1476-4687.
 - ⁵ Q.-G. Yang, D. Wang, and Q.-H. Wang, Physical Review B **108**, 1140505 (2023), ISSN 2469-9969.
 - ⁶ F. Lechermann, J. Gondolf, S. Bötzel, and I. M. Eremin, Physical Review B **108**, 1201121 (2023), ISSN 2469-9969.
 - ⁷ Y. Shen, M. Qin, and G.-M. Zhang, Chinese Physics Letters **40**, 127401 (2023), ISSN 1741-3540.
 - ⁸ Z. Liao, L. Chen, G. Duan, Y. Wang, C. Liu, R. Yu, and Q. Si, Physical Review B **108**, 214522 (2023), ISSN 2469-9969.
 - ⁹ Z. Ouyang, M. Gao, and Z.-Y. Lu, *Absence of phonon-mediated superconductivity in $\text{La}_3\text{Ni}_2\text{O}_7$ under pressure* (2024).
 - ¹⁰ H. Oh, B. Zhou, and Y.-H. Zhang, *Type ii t-j model in charge transfer regime in bilayer $\text{La}_3\text{Ni}_2\text{O}_7$ and trilayer $\text{La}_4\text{Ni}_3\text{O}_{10}$* (2024).
 - ¹¹ Y.-f. Yang, G.-M. Zhang, and F.-C. Zhang, Physical Review B **108**, 1201108 (2023), ISSN 2469-9969.
 - ¹² Q. Qin and Y.-f. Yang, Physical Review B **108**, 1140504 (2023), ISSN 2469-9969.
 - ¹³ Y.-H. Tian, Y. Chen, J.-M. Wang, R.-Q. He, and Z.-Y. Lu, *Correlation effects and concomitant two-orbital s_{\pm} -wave superconductivity in $\text{La}_3\text{Ni}_2\text{O}_7$ under high pressure* (2023).
 - ¹⁴ D.-C. Lu, M. Li, Z.-Y. Zeng, W. Hou, J. Wang, F. Yang, and Y.-Z. You, *Superconductivity from doping symmetric mass generation insulators: Application to $\text{La}_3\text{Ni}_2\text{O}_7$ under pressure* (2023).
 - ¹⁵ Z. Luo, B. Lv, M. Wang, W. Wú, and D.-X. Yao, *High- t_c superconductivity in $\text{La}_3\text{Ni}_2\text{O}_7$ based on the bilayer two-orbital t-j model* (2023).
 - ¹⁶ J.-X. Zhang, H.-K. Zhang, Y.-Z. You, and Z.-Y. Weng, *Strong pairing originated from an emergent \mathbb{Z}_2 berry phase in $\text{La}_3\text{Ni}_2\text{O}_7$* (2023).
 - ¹⁷ H. Yang, H. Oh, and Y.-H. Zhang, *Strong pairing from small fermi surface beyond weak coupling: Application to $\text{La}_3\text{Ni}_2\text{O}_7$* (2023).
 - ¹⁸ C. Lu, Z. Pan, F. Yang, and C. Wu, *Interplay of two e_g orbitals in superconducting $\text{La}_3\text{Ni}_2\text{O}_7$ under pressure* (2023).
 - ¹⁹ T. Kaneko, H. Sakakibara, M. Ochi, and K. Kuroki, Physical Review B **109**, 045154 (2024), ISSN 2469-9969.
 - ²⁰ H. Lange, L. Homeier, E. Demler, U. Schollwöck, F. Grusdt, and A. Bohrdt, *Feshbach resonance in a strongly repulsive bilayer model: a possible scenario for bilayer nickelate superconductors* (2023).
 - ²¹ S. Ryee, N. Witt, and T. O. Wehling, *Quenched pair breaking by interlayer correlations as a key to superconductivity in $\text{La}_3\text{Ni}_2\text{O}_7$* (2023).
 - ²² J. Chen, F. Yang, and W. Li, *Orbital-selective superconductivity in the pressurized bilayer nickelate $\text{La}_3\text{Ni}_2\text{O}_7$: An infinite projected entangled-pair state study* (2023).
 - ²³ H. Schlömer, U. Schollwöck, F. Grusdt, and A. Bohrdt, *Superconductivity in the pressurized nickelate $\text{La}_3\text{Ni}_2\text{O}_7$ in the vicinity of a bec-bcs crossover* (2023).
 - ²⁴ X.-Z. Qu, D.-W. Qu, W. Li, and G. Su, *Roles of hund's rule and hybridization in the two-orbital model for high- t_c superconductivity in the bilayer nickelate* (2023).
 - ²⁵ M. Kakoi, T. Kaneko, H. Sakakibara, M. Ochi, and K. Kuroki, *Pair correlations of the hybridized orbitals in a ladder model for the bilayer nickelate $\text{La}_3\text{Ni}_2\text{O}_7$* (2023).
 - ²⁶ S. Bötzel, F. Lechermann, J. Gondolf, and I. M. Eremin, Physical Review B **109**, 1180502 (2024), ISSN 2469-9969.
 - ²⁷ J. Zhan, Y. Gu, X. Wu, and J. Hu, *Cooperation between electron-phonon coupling and electronic interaction in bilayer nickelates $\text{La}_3\text{Ni}_2\text{O}_7$* (2024).
 - ²⁸ K. Jiang, Z. Wang, and F.-C. Zhang, Chinese Physics Letters **41**, 017402 (2024), ISSN 1741-3540.
 - ²⁹ Z. Wang, H.-J. Zhang, K. Jiang, and F.-C. Zhang, *Self-doped molecular mott insulator for bilayer high-temperature superconducting $\text{La}_3\text{Ni}_2\text{O}_7$* (2024).
 - ³⁰ X. Chen, J. Zhang, A. S. Thind, S. Sharma, H. LaBollita, G. Peterson, H. Zheng, D. P. Phelan, A. S. Botana, R. F. Klie, et al., Journal of the American Chemical Society **146**, 3640 (2024), ISSN 1520-5126.
 - ³¹ H. Wang, L. Chen, A. Rutherford, H. Zhou, and W. Xie, Inorganic Chemistry **63**, 5020 (2024), ISSN 1520-510X.
 - ³² P. Puphal, P. Reiss, N. Enderlein, Y.-M. Wu, G. Khaliullin, V. Sundaramurthy, T. Priessnitz, M. Knauff, L. Richter, M. Isobe, et al., *Unconventional crystal structure of the high-pressure superconductor $\text{La}_3\text{Ni}_2\text{O}_7$* (2023).
 - ³³ X. Chen, J. Choi, Z. Jiang, J. Mei, K. Jiang, J. Li, S. Agrestini, M. Garcia-Fernandez, X. Huang, H. Sun, et al., *Electronic and magnetic excitations in $\text{La}_3\text{Ni}_2\text{O}_7$* (2024).
 - ³⁴ Z. Dong, M. Huo, J. Li, J. Li, P. Li, H. Sun, L. Gu, Y. Lu, M. Wang, Y. Wang, et al., Nature (2024), ISSN 1476-4687.
 - ³⁵ R. J. Green, M. W. Haverkort, and G. A. Sawatzky, Physical Review B **94**, 195127 (2016), ISSN 2469-9969.
 - ³⁶ P. Kuiper, G. Kruijzinga, J. Ghijsen, G. A. Sawatzky, and H. Verweij, Physical Review Letters **62**, 221 (1989), ISSN 0031-9007.
 - ³⁷ V. J. Emery and G. Reiter, Physical Review B **38**, 4547 (1988), ISSN 0163-1829.
 - ³⁸ F. C. Zhang and T. M. Rice, Phys. Rev. B **41**, 7243 (1990), URL <https://link.aps.org/doi/10.1103/PhysRevB.41.7243>.
 - ³⁹ B. Lau, M. Berciu, and G. A. Sawatzky, Physical Review Letters **106**, 036401 (2011), ISSN 1079-7114.
 - ⁴⁰ Y. Zhang, L.-F. Lin, A. Moreo, and E. Dagotto, Physical Review B **108**, 1180510 (2023), ISSN 2469-9969.
 - ⁴¹ V. Pardo and W. E. Pickett, Physical Review B **83**, 245128 (2011), ISSN 1550-235X.
 - ⁴² Y. Gu, C. Le, Z. Yang, X. Wu, and J. Hu, *Effective model and pairing tendency in bilayer ni-based superconductor $\text{La}_3\text{Ni}_2\text{O}_7$* (2023).
 - ⁴³ H. Sakakibara, N. Kitamine, M. Ochi, and K. Kuroki, Physical Review Letters **132**, 106002 (2024), ISSN 1079-7114.
 - ⁴⁴ D. A. Shilenko and I. V. Leonov, Physical Review B **108**, 125105 (2023), ISSN 2469-9969.
 - ⁴⁵ X. Chen, P. Jiang, J. Li, Z. Zhong, and Y. Lu, *Critical charge and spin instabilities in superconducting $\text{La}_3\text{Ni}_2\text{O}_7$* (2023).
 - ⁴⁶ Y. Zhang, L.-F. Lin, A. Moreo, T. A. Maier, and E. Dagotto, Nature Communications **15** (2024), ISSN 2041-1723.
 - ⁴⁷ R. Jiang, J. Hou, Z. Fan, Z.-J. Lang, and W. Ku, Physical Review Letters **132**, 126503 (2024), ISSN 1079-7114.
 - ⁴⁸ B. Geisler, J. J. Hamlin, G. R. Stewart, R. G. Hennig, and P. J. Hirschfeld, *Structural transitions, octahedral rotations, and electronic properties of $\text{a}_3\text{Ni}_2\text{O}_7$ rare-earth nickelates under high pressure* (2023).

- ⁴⁹ H. LaBollita, V. Pardo, M. R. Norman, and A. S. Botana, *Electronic structure and magnetic properties of $la_3ni_2o_7$ under pressure: active role of the $ni-d_{x^2-y^2}$ orbitals* (2023).
- ⁵⁰ V. Christiansson, F. Petocchi, and P. Werner, *Physical Review Letters* **131**, 206501 (2023), ISSN 1079-7114.
- ⁵¹ Y. Wang, K. Jiang, Z. Wang, F.-C. Zhang, and J. Hu, *Physical Review B* **110**, 205122 (2024), ISSN 2469-9969.
- ⁵² Z. Ouyang, J.-M. Wang, J.-X. Wang, R.-Q. He, L. Huang, and Z.-Y. Lu, *Hund electronic correlation in $la_3ni_2o_7$ under high pressure* (2023).
- ⁵³ G. Heier, K. Park, and S. Y. Savrasov, *Physical Review B* **109**, 104508 (2024), ISSN 2469-9969.
- ⁵⁴ J. P. Perdew and Y. Wang, *Physical Review B* **45**, 13244 (1992), ISSN 1095-3795.
- ⁵⁵ V. I. Anisimov, I. V. Solovyev, M. A. Korotin, M. T. Czyżyk, and G. A. Sawatzky, *Physical Review B* **48**, 16929 (1993), ISSN 1095-3795.
- ⁵⁶ M. T. Czyżyk and G. A. Sawatzky, *Physical Review B* **49**, 14211 (1994), ISSN 1095-3795.
- ⁵⁷ G. Kotliar, S. Y. Savrasov, K. Haule, V. S. Oudovenko, O. Parcollet, and C. A. Marianetti, *Reviews of Modern Physics* **78**, 865 (2006), ISSN 1539-0756.
- ⁵⁸ K. Foyevtsova, I. Elfimov, and G. A. Sawatzky, *Physical Review B* **108**, 205124 (2023), ISSN 2469-9969.
- ⁵⁹ K. Foyevtsova and G. A. Sawatzky, *Journal of Modern Physics* **10**, 953 (2019), ISSN 2153-120X.
- ⁶⁰ G. Jiang, C. Qin, K. Foyevtsova, L. Si, M. Berciu, G. A. Sawatzky, and M. Jiang, *Intertwined charge and spin instability of $la_3ni_2o_7$* (2025), 2410.15649, URL <https://arxiv.org/abs/2410.15649>.
- ⁶¹ A. D. Becke, *The Journal of Chemical Physics* **98**, 1372 (1993), ISSN 1089-7690.
- ⁶² Z. Liu, H. Sun, M. Huo, X. Ma, Y. Ji, E. Yi, L. Li, H. Liu, J. Yu, Z. Zhang, et al., *Sci. China Phys. Mech. Astron.* **66**, 217411 (2023).
- ⁶³ M. Kakoi, T. Oi, Y. Ohshita, M. Yashima, K. Kuroki, T. Kato, H. Takahashi, S. Ishiwata, Y. Adachi, N. Hatada, et al., *Multiband metallic ground state in multilayered nickelates $la_3ni_2o_7$ and $la_4ni_3o_{10}$ probed by ^{139}la -nmr at ambient pressure* (2023).
- ⁶⁴ Z. Dan, Y. Zhou, M. Huo, Y. Wang, L. Nie, M. Wang, T. Wu, and X. Chen, *Spin-density-wave transition in double-layer nickelate $la_3ni_2o_7$* (2024).
- ⁶⁵ G. Kresse and J. Furthmüller, *Computational Materials Science* **6**, 15 (1996), ISSN 0927-0256.
- ⁶⁶ J. Heyd, G. E. Scuseria, and M. Ernzerhof, *The Journal of Chemical Physics* **118**, 8207 (2003), ISSN 1089-7690.
- ⁶⁷ J. P. Perdew, K. Burke, and M. Ernzerhof, *Physical Review Letters* **77**, 3865 (1996), ISSN 1079-7114.
- ⁶⁸ K. Chen, X. Liu, J. Jiao, M. Zou, Y. Luo, Q. Wu, N. Zhang, Y. Guo, and L. Shu, *Evidence of spin density waves in $la_3ni_2o_{7-\delta}$* (2023).
- ⁶⁹ A. I. Liechtenstein, V. I. Anisimov, and J. Zaanen, *Physical Review B* **52**, R5467 (1995), ISSN 1095-3795.
- ⁷⁰ K. Momma and F. Izumi, *Journal of Applied Crystallography* **41**, 653 (2008), ISSN 0021-8898.
- ⁷¹ I. Plokhikh, T. J. Hicken, L. Keller, V. Pomjakushin, S. H. Moody, P. Foury-Leylekian, J. J. Krieger, H. Luetkens, Z. Guguchia, R. Khasanov, et al., *Unraveling spin density wave order in layered nickelates $La_3Ni_2O_7$ and $La_2PrNi_2O_7$ via neutron diffraction* (2025), 2503.05287, URL <https://arxiv.org/abs/2503.05287>.